Coulomb drag between parallel two-dimensional electron systems

Antti-Pekka Jauho*
Nordita, Blegdamsvej 17, Copenhagen 2100 Ø, Denmark

Henrik Smith
Physics Laboratory, H. C. Ørsted Institute, Universitetsparken 5, Copenhagen 2100 Ø, Denmark
(Received 21 April 1992; revised manuscript received 2 November 1992)

The Coulomb contribution to the temperature-dependent rate of momentum transfer, $1/\tau_D$, between two electron systems in parallel layers is determined by setting up two coupled Boltzmann equations, with the boundary condition that no current flows in the layer where an induced voltage is measured. The effective Coulomb interaction between the layers is determined self-consistently, allowing for the finite thickness of the layers. As $T\rightarrow 0$, we find that $1/\tau_D T^2$ approaches a constant value. At higher temperatures, $1/\tau_D T^2$ exhibits a maximum at $T=T_{\max}$ and then decreases as $1/T$ with increasing temperature. The value of $T_{\max}$ depends on the layer separation d according to $T_{\max}\propto d^{-\alpha}$, where $\alpha\simeq 0.8$. The overall magnitude of the calculated $1/\tau_D$ is approximately one-half of the results of a recent experiment, suggesting that other mechanisms of momentum transfer may be important.

I. INTRODUCTION

It is well known that the electron-electron scattering rate $1/\tau(\varepsilon)$ in a three-dimensional electron gas at zero temperature depends on the electron energy ε according to $1/\tau(\varepsilon)\propto(\varepsilon-\mu)^2$, where μ is the chemical potential.[1] At finite temperatures this characteristic energy dependence yields relaxation rates that are proportional to T^2. The effects of electron-electron scattering on the transport properties of ordinary metals is usually weak compared to the competing effect of electron-impurity and electron-phonon scattering. The T^2 dependence associated with electron-electron scattering has been observed in metals at relatively high temperatures by measuring deviations from the Wiedemann-Franz-Lorenz law (for a discussion of this and other consequences of electron-electron scattering, see, e.g. Ref. 2). At low temperatures the effects of electron-electron scattering on various transport properties are often difficult to separate from the effects of other inelastic processes. The phase breaking due to electron-electron scattering has important consequences for the localization phenomena occurring in disordered systems and it has been investigated extensively in this context.[3]

The characteristic energy dependence of the electron-electron scattering rate is due to the phase-space restrictions that apply to the mutual scattering of particles in a nearly degenerate gas. These restrictions are different in two and in three dimensions. For a two-dimensional electron gas one finds that the scattering rate at zero temperature is proportional to $(\varepsilon-\mu)^2\ln|\varepsilon-\mu|$, as shown by Hodges, Smith, and Wilkins[4] and, independently, by Chaplik.[5] At finite temperatures the corresponding relaxation rates become proportional to $T^2\ln T$. The nonanalytic temperature dependence can be traced to a logarithmic singularity for values of the momentum transfer $\hbar q$, which are near either zero or $2\hbar k_F$, where k_F is the Fermi wave vector. The logarithmic energy dependence $(\varepsilon-\mu)^2\ln|\varepsilon-\mu|$ was recently confirmed experimentally[6] by measurements of quantum interference in a two-dimensional electron gas.

In a recent experiment Gramila *et al.*[7] measured the mutual friction between two parallel two-dimensional electron systems as a function of the temperature and the distance between the two layers. The systems investigated consisted of modulation-doped GaAs/Al_xGa_{1-x}As double quantum wells, grown by molecular-beam epitaxy. The observed frictional drag was interpreted as being due to the Coulomb interaction between the two separate electron systems. Gramila *et al.*[7] also performed a calculation of the drag in the low-temperature limit, and found the rate of momentum transfer to be proportional to T^2. Although the overall temperature dependence of their calculated rate was in qualitative agreement with experiment, there remained significant differences, in particular for samples with large values of the layer separation.[8]

The purpose of the present paper is to investigate the Coulomb drag problem in detail by calculating the rate of momentum transfer as a function of temperature. In the limit of very low temperatures we find that the rate of momentum transfer is proportional to T^2, in agreement with the result obtained in Ref. 7. At temperatures which are somewhat higher (but still small compared to the Fermi temperature T_F) our calculated temperature dependence differs from T^2. As we shall see, the deviation from the T^2 dependence is in qualitative, but not quantitative, agreement with the one observed experimentally in Ref. 7, where the momentum relaxation rate divided by T^2 was found to exhibit a maximum around $T=2$ K, which is about 30 times less than T_F.

Although the indirect electron-electron interaction caused by the virtual exchange of phonons may also affect the observed friction,[7,8] the scope of the present work is limited to evaluating the temperature dependence arising from the Coulomb interaction and comparing the calculated relaxation rate with the one measured experimentally. Our formulation is, however, sufficiently general that other coupling mechanisms besides the direct

Coulomb interaction may be incorporated.

The possibility of observing the Coulomb drag effect in heterostructures was suggested by Price.[9] A theoretical formulation of the drag problem was given by Pogrebinskii.[10] The effect has been considered in both one-, two-, and three-dimensional systems by a number of different authors, cf. Refs. 11–16. Most of these calculations treat only high- or low-temperature limits, and to our knowledge the full temperature dependence of the Coulomb drag has not been considered before. Momentum transfer between two coupled electron-hole gases was studied recently by Sivan, Solomon, and Shtrikman.[17]

The plan of the paper is as follows. In Sec. II we define the drag resistivity and the associated momentum relaxation rate in terms of experimentally observable quantities. The theoretical model used for calculating the momentum relaxation rate is treated in Sec. III, where we set up the two coupled Boltzmann equations and derive a general expression for the momentum relaxation rate. We also discuss the screening of the Coulomb interaction between electrons in the two layers. The resulting effective interaction enters our expression for the momentum relaxation rate, which in general must be evaluated numerically. In Sec. IV we perform an analytic evaluation of the rate of momentum relaxation at very low temperatures and exhibit the results of the numerical calculation at arbitrary temperatures. The theoretical results are compared to the measured momentum relaxation rate, in regard to its absolute magnitude as well as its dependence on temperature and layer separation. The detailed derivation of the screened Coulomb interaction is deferred to the Appendix.

II. DRAG RESISTIVITY

Let us consider two parallel layers each containing a two-dimensional gas of electrons, as illustrated in Fig. 1. The perpendicular distance between the midpoints of the two layers is denoted by d. In the experiment performed by Gramila *et al.*[7] a current I_2 is driven along layer 2, and one measures the voltage difference V_1 which is induced in layer 1 under the condition that no current flows in this layer. The current per unit width, j_2, in layer 2 is given by $j_2 = I_2/W$, while the magnitude of the electric field strength, which prevents the electrons in layer 1 from being dragged along by the current in layer 2, is $E_1 = V_1/l$. Here W is the width of layer 2, while l denotes the distance between the potential probes shown in Fig. 1. The drag resistivity ρ_D is then defined by

$$\rho_D = \frac{E_1}{j_2} = \frac{WV_1}{I_2 l} \ . \tag{1}$$

Following Ref. 7 it is convenient to translate the drag resistivity into a momentum relaxation rate $1/\tau_D$ by defining the drift velocity u_2 according to

$$j_2 = n_2 e u_2 \ , \tag{2}$$

where n_2 is the number of electrons per unit area in layer 2, while e is the elementary charge. Experimentally, the electric field E_1 is found to be proportional to u_2. The coefficient relating the two quantities is the drag mobility μ_D, which is defined by

$$\mu_D = \frac{u_2}{E_1} \ . \tag{3}$$

The mobility μ_D may in turn be expressed in terms of the momentum relaxation rate $1/\tau_D$, defined according to

$$\mu_D = \frac{e}{m}\tau_D \ , \tag{4}$$

where m is the effective mass of the conduction electrons (in the case of $Al_xGa_{1-x}As/GaAs$, the effective mass m is 0.067 times the electron mass m_e). The drag resistivity ρ_D, which has the dimension of a resistance, may thus be written as

$$\rho_D = \frac{m}{n_2 e^2 \tau_D} \ . \tag{5}$$

In summary, the ratio between the observed voltage V_1 and the imposed current I_2 is expressed in terms of the drag resistivity ρ_D by the definition

$$\frac{V_1}{I_2} = \frac{l}{W}\rho_D \ , \tag{6}$$

where ρ_D according to (5) may be written in terms of the momentum relaxation rate $1/\tau_D$. Equations (5) and (6) are simply a definition of a convenient quantity τ_D, which we determine in the following section as a function of the temperature T and the distance d separating the two layers, starting from the Boltzmann equation for the distribution function of the electrons.

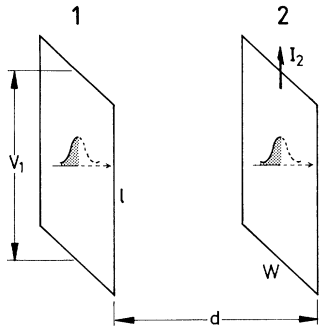

FIG. 1. Schematic drawing of the experimental geometry. The current I_2 is driven through layer 2, and the voltage difference V_1 is induced in layer 1. Also illustrated is the finite extent of the wave functions in the direction perpendicular to the layers.

III. THE MOMENTUM RELAXATION RATE

The momentum relaxation rate is determined by using the linearized Boltzmann equation to derive a balance equation between the induced electric field and the drag due to the drive current. In the presence of an electric

field $\mathbf{E}_1$ this linearized Boltzmann equation is

$$\dot{\mathbf{k}}_1 \cdot \frac{\partial f_1^0}{\partial \mathbf{k}_1} = \left[\frac{\partial f_1}{\partial t} \right]_{\text{coll}} , \tag{7}$$

where

$$\hbar \dot{\mathbf{k}}_1 = -e\mathbf{E}_1 , \tag{8}$$

while f^0 is the equilibrium distribution function (we label quantities referring to layer 1 by 1, 1', etc. and similarly for layer 2). The linearized collision integral is

$$\left[\frac{\partial f_1}{\partial t} \right]_{\text{coll}} = -\sum_{\sigma_2,\sigma_{1'},\sigma_{2'}} \int \frac{d\mathbf{k}_2}{(2\pi)^2} \int \frac{d\mathbf{k}_{1'}}{(2\pi)^2} w(1,2;1',2')(\psi_1+\psi_2-\psi_{1'}-\psi_{2'}) f_1^0 f_2^0 (1-f_{1'}^0)(1-f_{2'}^0)\delta(\varepsilon_1+\varepsilon_2-\varepsilon_{1'}-\varepsilon_{2'}) . \tag{9}$$

Here the function $w(1,2;1',2')$ determines the probability that two electrons in states $\mathbf{k}_1\sigma_1$ and $\mathbf{k}_2\sigma_2$ will scatter to $\mathbf{k}_{1'}\sigma_{1'}$ and $\mathbf{k}_{2'}\sigma_{2'}$. Due to momentum conservation, we have $\mathbf{k}_{2'}=\mathbf{k}_1+\mathbf{k}_2-\mathbf{k}_{1'}$. In the Born approximation w is proportional to the square of the Fourier transform of the effective interaction as specified below. The deviation function ψ has been introduced by the definition

$$f-f^0=f^0(1-f^0)\psi , \tag{10}$$

implying that ψ vanishes in equilibrium.

The current flowing in layer 2 is assumed to be limited by impurity scattering, corresponding to the deviation function

$$\psi_2 = -\frac{1}{kT}\tau_2 e v_{2x} E_2 , \tag{11}$$

where $\mathbf{E}_2$ is the electric field in layer 2, directed along the x axis, and τ_2 is a (energy-independent) momentum relaxation time, which determines the electron mobility μ_2 according to $\mu_2=e\tau_2/m$. Since no current is flowing in layer 1, the electron distribution in this layer is taken to be the equilibrium one, corresponding to $\psi_1=\psi_{1'}=0$. According to (7)–(9) the electric field $\mathbf{E}_1$ then balances the drag resulting from the fact that ψ_2 and $\psi_{2'}$ are nonzero. In order to determine E_1 we insert the nonequilibrium distribution function given by (11) into (9). Due to momentum conservation we have

$$v_{2x}-v_{2'x}=v_{1'x}-v_{1x} , \tag{12}$$

since the effective masses m are assumed to be identical in the two layers. We now multiply both sides of (7) by k_{1x} and sum over the states $\mathbf{k}_1\sigma_1$. This yields

$$2\int \frac{d\mathbf{k}_1}{(2\pi)^2} k_{1x} \frac{(-e)E_1}{\hbar} \frac{\partial}{\partial k_{1x}} f^0(\varepsilon_1) = \sum_{\sigma_1} \int \frac{d\mathbf{k}_1}{(2\pi)^2} k_{1x} \left[\frac{\partial f_1}{\partial t} \right]_{\text{coll}} . \tag{13}$$

The left-hand side of (13) then becomes $eE_1 n_1/\hbar$ after use of partial integration, with n_1 being the electron density, which is related to the Fermi wave vector k_F according to

$$n_1 = \frac{k_F^2}{2\pi} . \tag{14}$$

We assume in this section that the electron number density is the same in the two layers, $n_1=n_2$. It is straightforward to generalize our treatment to the case where the two densities differ.

The right-hand side of (13) may be simplified, as the quantity $k_{1x}(k_{1'x}-k_{1x})$ in the integrand may be replaced by $-(k_{1'x}-k_{1x})^2/2$, because of the symmetry of the remaining part of the integrand with respect to the interchange of 1 and 1'. Furthermore, since the calculated momentum relaxation rate is independent of whether the electric field is taken to be along the x or the y axis, we add the corresponding contributions and divide by 2, resulting in the replacement of $(k_{1'x}-k_{1x})^2/2$ by $q^2/4$, where $\mathbf{q}$ is the wave-vector transfer given by

$$\mathbf{q}=\mathbf{k}_{1'}-\mathbf{k}_1 . \tag{15}$$

This allows us to further simplify the right-hand side of (13):

$$\sum_{\sigma_1} \int \frac{d\mathbf{k}_1}{(2\pi)^2} k_{1x} \left[\frac{\partial f_1}{\partial t} \right]_{\text{coll}} = -\frac{e\hbar E_2 \tau_2}{4mkT} \sum_{\sigma_1,\sigma_2,\sigma_{1'},\sigma_{2'}} \int \frac{d\mathbf{k}_1}{(2\pi)^2} \int \frac{d\mathbf{k}_2}{(2\pi)^2} \int \frac{d\mathbf{k}_1'}{(2\pi)^2} w(1,2;1',2') q^2 f_1^0 f_2^0 (1-f_{1'}^0) \times (1-f_{2'}^0)\delta(\varepsilon_1+\varepsilon_2-\varepsilon_{1'}-\varepsilon_{2'}) . \tag{16}$$

We shall make the simplifying assumption that w only depends on $\mathbf{q}$ (and possibly $\varepsilon_1-\varepsilon_{1'}$). Then we introduce $\mathbf{q}$ as an integration variable in (16). It is convenient[18] to express (16) in terms of the two-dimensional susceptibility function $\chi(q,\omega)$, defined by

$$\chi(q,\omega)=-\int \frac{d\mathbf{k}_1}{(2\pi)^2}\frac{f^0(\varepsilon_1)-f^0(\varepsilon_{1'})}{\varepsilon_1-\varepsilon_{1'}+\hbar\omega+i\delta} . \tag{17}$$

The imaginary part of the susceptibility, $\mathrm{Im}\chi$, is given at zero temperature by

$$\mathrm{Im}\chi(q,\omega)=\begin{cases}\dfrac{mk_F}{2\pi\hbar^2 q}\left\{\left[1-\left[\dfrac{\omega}{v_F q}-\dfrac{q}{2k_F}\right]^2\right]^{1/2}-\left[1-\left[\dfrac{\omega}{v_F q}+\dfrac{q}{2k_F}\right]^2\right]^{1/2}\right\} & \text{for } q<2k_F\ ,\ 0<\omega<v_F q(1-q/2k_F)\\ \dfrac{mk_F}{2\pi\hbar^2 q}\left[1-\left[\dfrac{\omega}{v_F q}-\dfrac{q}{2k_F}\right]^2\right]^{1/2} & \text{for } q<2k_F\ ,\ v_F q(1-q/2k_F)<\omega<v_F q(1+q/2k_F)\\ \dfrac{mk_F}{2\pi\hbar^2 q}\left[1-\left[\dfrac{\omega}{v_F q}-\dfrac{q}{2k_F}\right]^2\right]^{1/2} & \text{for } q>2k_F\ ,\ v_F q(-1+q/2k_F)<\omega<v_F q(1+q/2k_F)\\ 0 \text{ otherwise} . & \end{cases} \tag{18}$$

Strictly speaking we should here use the finite-temperature expression[19] for $\mathrm{Im}\chi$. This, however, would only affect the momentum relaxation rate to higher order in T/T_F, and we may therefore use the zero-temperature expression, since we are not interested in variations on the scale of the Fermi temperature, but on a much smaller temperature scale set by the distance between the two layers. As we shall see in Sec. IV below, this characteristic temperature scale is given approximately by $T_F/(k_F d)^{\alpha}$, where $\alpha\simeq 0.8$.

By using the identities

$$\delta(\varepsilon_1+\varepsilon_2-\varepsilon_{1'}-\varepsilon_{2'})=\hbar\int_{-\infty}^{\infty} d\omega\,\delta(\varepsilon_1-\varepsilon_{1'}-\hbar\omega)\delta(\varepsilon_2-\varepsilon_{2'}+\hbar\omega) \tag{19}$$

and

$$f^0(\varepsilon)[1-f^0(\varepsilon+\hbar\omega)]=[f^0(\varepsilon)-f^0(\varepsilon+\hbar\omega)]/[1-\exp(-\hbar\omega/kT)] \tag{20}$$

we may transform the expression (16) into

$$\sum_{\sigma_1}\int\frac{d\mathbf{k}_1}{(2\pi)^2}k_{1x}\left[\frac{\partial f_1}{\partial t}\right]_{\mathrm{coll}}=-\frac{e\hbar^2E_2\tau_2}{8\pi^2mkT}\sum_{\sigma_1,\sigma_2,\sigma_{1'},\sigma_{2'}}\int\frac{d\mathbf{q}}{(2\pi)^2}\int_0^{\infty}d\omega[\mathrm{Im}\chi(q,\omega)]^2 w(1,2;1',2')\frac{q^2}{\sinh^2(\hbar\omega/2kT)} , \tag{21}$$

by using that the integrand is an even function of ω.

To proceed further we must specify the effective interaction. Our starting point is the direct Coulomb interaction between electrons in each layer, suitably modified by the screening in the two-dimensional electron gas. For simplicity we assume static screening, treated in the Thomas-Fermi approximation, which in two dimensions yields the same result as the random-phase approximation provided the wave-vector transfer in the collisions between electrons is less than twice the Fermi wave vector. The effective interaction is obtained by solving Poisson's equation for the potential due to a point source situated in one of the two layers. When the wave-vector transfer is much larger than both the inverse distance between the two layers and the Thomas-Fermi screening wave vector, the Fourier transform $e\phi(q)$ of the effective interaction reduces to that of the bare Coulomb interaction between charge densities localized at the two quantum wells. In the general case treated in the Appendix, ϕ is shown to be of the form

$$e\phi(q)=\frac{2\pi e^2}{\kappa q_{\mathrm{TF}}}\frac{q/q_{\mathrm{TF}}}{g_{12}^{-1}(g_{11}+q/q_{\mathrm{TF}})^2-g_{12}} . \tag{22}$$

Here $g_{11}=-2qG_{11}$ and $g_{12}=-2qG_{12}$ are functions of q, where G_{12} and G_{11} are form factors given by (A16) and (A17), while q_{TF} is the Thomas-Fermi screening wave vector appropriate to two dimensions,

$$q_{\mathrm{TF}}=\frac{2me^2}{\kappa\hbar^2} , \tag{23}$$

κ being the dielectric constant (for GaAs $\kappa\simeq 13$).

The simplest case to consider is that in which the width L of the quantum wells is effectively zero, which corresponds to treating the two layers as mathematical planes. Then the functions g_{11} and g_{12} reduce to

$$g_{11}=1\ ,\quad g_{12}=e^{-qd} . \tag{24}$$

We may take into account the finite width of the quantum wells by assuming a specific form of the electron wave function in the direction perpendicular to the layers. If the latter is approximated by the ground-state wave function of an infinitely deep well, the functions $G_{11}(q)$ and $G_{12}(q)$ become those given by (A16) and (A17).

When the collision probability is obtained from the effective interaction by use of the Born approximation (or, equivalently, the golden rule), we get

$$\sum_{\sigma_1,\sigma_2,\sigma_{1'},\sigma_{2'}} w(1,2;1',2')=\frac{2\pi}{\hbar}4|e\phi(q)|^2 . \tag{25}$$

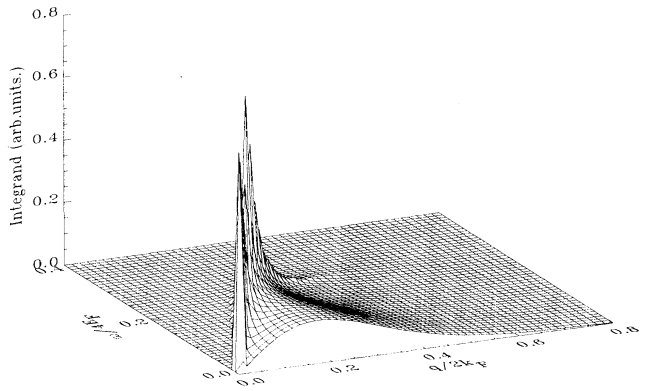

FIG. 2. The q and ω dependence of the integrand in (27) for $T=10$ K.

The factor of 4 arises from doing the spin summations, taking into account that w vanishes when $\sigma_{1'}\neq\sigma_1$ and $\sigma_{2'}\neq\sigma_2$.

Collecting these results and using (2)–(4) together with $u_2=e\tau_2 E_2/m$ we can express the ratio between the electric fields in layers 1 and 2 in terms of the momentum relaxation rate $1/\tau_D$ according to

$$\frac{E_1}{E_2}=\frac{\tau_2}{\tau_D} , \tag{26}$$

where

$$\frac{1}{\tau_D}=\frac{\hbar^2}{2\pi^2 n_1 mkT}\int_0^\infty dq\int_0^\infty d\omega\, q^3|e\phi(q)|^2[\mathrm{Im}\chi(q,\omega)]^2 \times\frac{1}{\sinh^2(\hbar\omega/2kT)} . \tag{27}$$

Note that the factor q^2, which enters the momentum relaxation rate under consideration, removes the singularity at small q.

We have exhibited in Fig. 2 the q and ω dependence of the integrand in (27). Note that the integrand vanishes for $q=0$, while it is nonzero for $\omega\to 0$, $q\neq 0$, since $\mathrm{Im}\chi$ depends linearly on ω for small values of ω.[20]

The remaining task is now to carry out the integrations in (27), which we shall discuss in the following section.

IV. RESULTS AND DISCUSSION

In this concluding section we shall first consider the limit of very low temperatures, in which an analytic result may be extracted. Then we exhibit the results of our numerical calculation and compare with the experiments of Ref. 7.

A. The temperature-dependent rate of momentum relaxation

At sufficiently low temperatures we may approximate $\mathrm{Im}\chi$ by its low-frequency expansion, $\mathrm{Im}\chi \simeq m^2\omega/2\pi\hbar^3 qk_F$, valid for $q\ll k_F$. This allows one to complete the integration over ω, since

$$\int_0^\infty dx\frac{x^p}{4\sinh^2 x/2}=p!\zeta(p) . \tag{28}$$

The remaining integral over q involves the interaction matrix element $\phi(q)$, which is determined self-consistently in the Appendix. For simplicity we assume for the moment that the width L of the two layers may be set equal to zero (cf. Fig. 6, in which the effect of a finite layer thickness is illustrated), corresponding to the expression (A18),

$$e\phi(q)=\frac{2\pi e^2}{\kappa}\frac{q}{2q_{\mathrm{TF}}^2\sinh qd+(2qq_{\mathrm{TF}}+q^2)\exp qd} . \tag{29}$$

Since the important contributions from the q integration come from the region, in which q is comparable to or smaller than d^{-1}, and since d^{-1} is much smaller than both k_F and q_{TF} under the experimental conditions of Ref. 7, we may neglect the second term in the denominator of (29) and thus use the simple form

$$e\phi(q)=\frac{\pi e^2}{\kappa}\frac{q}{q_{\mathrm{TF}}^2\sinh qd} . \tag{30}$$

The final integration over q may now be carried out, using (28). This results in

$$\frac{1}{\tau_D}=\frac{\zeta(3)\pi}{16}\frac{k^2T^2}{\hbar\varepsilon_F}\frac{1}{(k_Fd)^2}\frac{1}{(q_{\mathrm{TF}}d)^2} . \tag{31}$$

Our low-temperature result (31) agrees with Ref. 7 apart from being a factor of 2 larger.

The quadratic temperature dependence given by (31) only applies to the low-temperature limit. At higher temperatures the integration must be carried out numerically. In the following we present a set of curves that illustrate the behavior of $1/\tau_D$ as a function of temperature and layer separation. In Fig. 3 we plot $1/\tau_D T^2$ as a function of temperature for two different values of the layer separation, $d=375$ and 425 Å, with the parameter L describing our model wave functions taken to be $L=200$ Å, appropriate to the experiments reported in Ref. 7. Note that $1/\tau_D T^2$ at higher temperatures decreases with

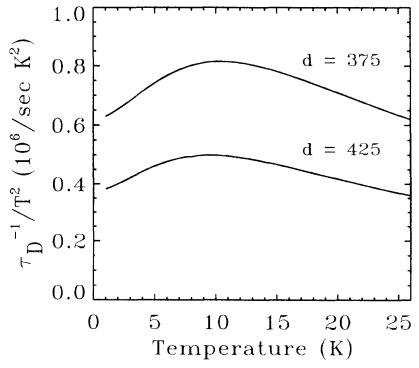

FIG. 3. The calculated values of $1/\tau_D T^2$ as functions of temperature, for the parameters $d=375$ and 425 Å appropriate to the experiment of Gramila *et al.* (Ref. 7). The value of L is 200 Å.

increasing temperature. By performing a high-temperature expansion (with the restriction that $T \ll T_F$) of (27), using $1/\sinh^2(\hbar\omega/2kT) \simeq 4k^2T^2/\hbar^2\omega^2 - \frac{1}{3}$, one finds that $1/\tau_D \propto T - \text{const}/T$, which is consistent with the observed fall-off at higher temperatures.[7]

To gain a better understanding of the physics underlying the nonmonotonic temperature dependence of $1/\tau_D T^2$, we rewrite Eq. (27) as

$$1/\tau_D T^2 = \int_0^\infty dq\, q|e\phi(q)|^2 F_T(q) , \tag{32}$$

where $F_T(q)$ is the result of the ω integration in (27). The two factors in the q integral have different physical origins: the ϕ term describes the q dependence of the interaction, while the $F_T(q)$ piece is related to the phase space corresponding to momentum transfer $\hbar q$; these two terms are plotted in Fig. 4. The function $F_T(q)$ is strongly temperature dependent, with a maximum which broadens and moves towards higher temperatures, as the temperature is increased. This behavior is a consequence of the interplay of the ω dependence of the thermal factor $\sinh^2(\hbar\omega/2kT)/T^3$, and the susceptibility function $q^2\mathrm{Im}^2\chi(q,\omega)$. At a certain temperature ($T = 10$ K in the present example), the maxima of $q|e\phi(q)|^2$ and $F_T(q)$ coincide, the interaction term and the phase-space term have a maximal overlap, and a maximum in the calculated value of $1/\tau_D T^2$ results.

In Fig. 5 the dependence of $d^4/\tau_D T^2$ on T is plotted for three different values of d. The curves illustrate that the momentum relaxation rate is proportional to d^{-4} only in the low-temperature limit. Note that the temperature $T_{\max}$, at which the curves have their maximum, shifts to lower temperatures when d is increased. In the $T \to 0$ limit, the analytic formula (31) gives $\tau_D^{-1} d^4/T^2 \to 1.38 \times 10^{-24}$ m^4/K^{2}s, which is slightly larger than the extrapolated value from Fig. 5. This result can be understood by examining Fig. 7, where one observes that the approximate effective interaction (30) is slightly larger than the full expression (22) used in the numerical calculation of Fig. 5.

The general shape of the curves depicted in Fig. 5 can also be understood based on Fig. 4. For an increasing layer spacing d, the maximum of $q|e\phi(q)|^2$ moves towards smaller q's, and hence the maximum in $1/\tau_D T^2$ moves towards lower temperatures.

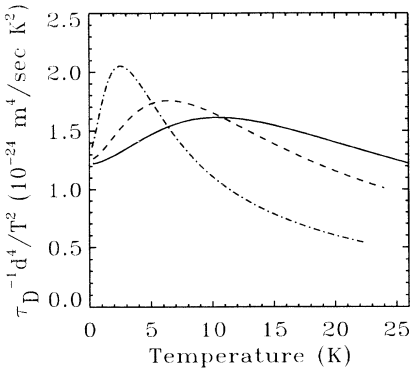

FIG. 5. The curves show the dependence of the scaled quantity $d^4/\tau_D T^2$ on temperature for three different choices of d: 375 Å (full curve), 700 Å (dashed curve), and 2100 Å (dot-dashed curve). The value of L is 200 Å.

Our numerical calculation shows that $T_{\max}$ is approximately proportional to $d^{-\alpha}$, where α is close to 0.8. This power-law behavior is illustrated in Fig. 6 for two different choices of the parameter L. The exponents obtained from the fit to a power law are nearly the same: $\alpha = 0.81$ and 0.76 for $L = 200$ and 1 Å, respectively. Finally we show in Fig. 7 how $|\phi(q)|^2$ depends on q, for different forms of the effective interaction considered in the Appendix.

B. Comparison with experiment

The experimental data obtained in Ref. 7 have a form similar to our theoretical curves in Fig. 3, but the temperature at which $1/\tau_D T^2$ has its maximum is significantly less, about 2.5 K in the experiment of Ref. 7. The Fermi temperature corresponding to the experimental value of

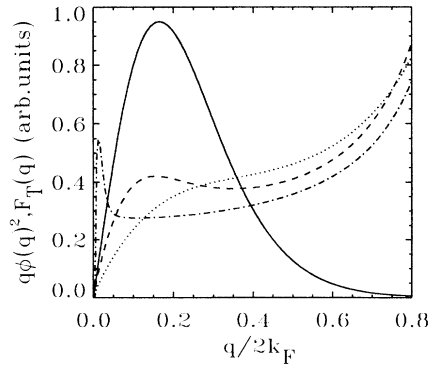

FIG. 4. The interaction term $q|e\phi(q)|^2$ (full curve; see also Fig. 7), and the phase-space term $F_T(q)$ for temperatures $T = 1$ K (dot-dashed curve), $T = 10$ K (dashed curve), and $T = 20$ K (dotted curve).

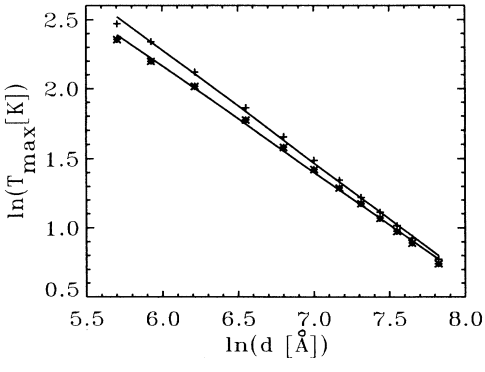

FIG. 6. The dependence of $T_{\max}$ on layer separation d for two different L values: $L = 200$ Å (crosses) and $L = 1$ Å (asterisks). The fitted values of the exponent α are 0.81 and 0.76, respectively.

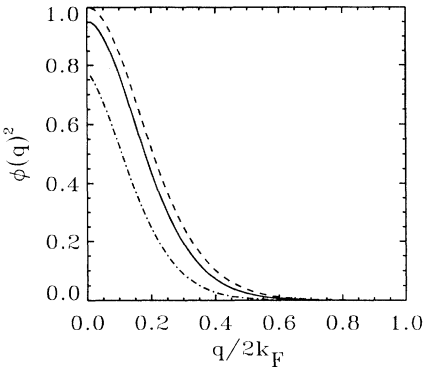

FIG. 7. The square of the matrix element, $|\phi(q)|^2$, as a function of momentum transfer. The full curve is obtained from (22), the dashed curve from (30), and the dot-dashed curve from (29). The units have been chosen such that $|\phi(q=0)|^2$ is unity for the dashed curve.

the number of electrons per unit area is 62 K. The maximum of the theoretical curves occurs around 10 K for the values of d shown in Fig. 3. Furthermore the observed rate is about a factor of 2 larger than our calculated values, suggesting that other mechanisms of momentum transfer may be important.

The expression (27) for the momentum relaxation rate may readily be generalized to the case where the densities and masses of the two systems of charge carriers differ. The experiment by Sivan, Solomon, and Shtrikman[17] involves a hole gas coupled to an electron gas. Since the hole mass is nearly seven times larger than the electron mass, the Fermi temperature $T_{F,h}$ for the holes is typically much less than the Fermi temperature $T_{F,e}$ for the electrons. This allows one to identify a temperature regime in which the electrons can be treated as a degenerate gas, while the holes behave as classical particles ($T_{F,h} \ll T \ll T_{F,e}$). Under such conditions one finds from (27) that the drag resistivity is

$$\rho_D = \frac{\pi^5}{960}\frac{T^2}{T_{F,e}^2}\frac{k_{F,e}}{q_{\mathrm{TF},e}^2 k_{F,h}^4 d^5}\frac{h}{e^2} . \tag{33}$$

In obtaining this result we have used the interaction (30) with $q_{\mathrm{TF},h}$ replaced by the classical expression $2\pi n_h e^2/\kappa kT$. Further, Imχ for the holes was evaluated in the classical limit, i.e., using Maxwell-Boltzmann distribution functions rather than Fermi-Dirac distributions. At $T=10$ K and for densities $n_e = 2\times 10^{11}$ cm^{-2} and $n_h = 5\times 10^{10}$ cm^{-2}, this yields $\rho_D \simeq 4\ \Omega$, while the observed value[17] of ρ_D is about 10 Ω at this temperature. We stress that the result (33) is derived under the condition that the electrons are completely degenerate, and the holes behave as classical particles. A more detailed comparison with the experimental results of Ref. 17 requires a numerical evaluation of (27), taking into account the full temperature dependence of the susceptibility function (18).

V. CONCLUSION

In this paper we have considered the rate of momentum transfer between two nearby electron gases, which are coupled via the screened Coulomb interaction. This system is of particular interest, because it provides a way of probing electron-electron interactions in two dimensions, which play a crucial role in many problems of current interest. It is well known that going from three to two dimensions may change qualitatively predictions based on phase-space arguments, the classical example being the logarithmic energy, or temperature, dependence of the electron lifetime. These effects can be related mathematically to logarithmic singularities in the phase-space integral, which determines the lifetime, or scattering rate. The phase space corresponding to the momentum transfer rate is different from the phase space related to the lifetime: the singularity corresponding to small momentum transfer is removed, and the $2k_F$ singularity is strongly suppressed due to the effective interaction, which decays exponentially for large momentum transfer. Thus it might seem that there is no reason to expect deviations from a T^2 temperature dependence. It was therefore a significant surprise when recent measurements revealed a nonmonotonic temperature dependence of the momentum transfer rate (when scaled by T^2). To account quantitatively for the experimental observations, it is likely that other mechanisms than the direct Coulomb coupling must be considered. However, as we have shown in this paper, the Coulomb coupling itself yields a nontrivial temperature dependence, which bears a clear resemblance to the one observed experimentally.

ACKNOWLEDGMENT

We thank J. P. Eisenstein for correspondence.

APPENDIX: THE EFFECTIVE COULOMB INTERACTION

The momentum relaxation rate depends on the effective Coulomb interaction between the electrons in the two planes. We shall now determine this interaction, starting from the Poisson equation and treating the screening in the Thomas-Fermi approximation.

The collision probability entering the Boltzmann equation is determined by matrix elements $\langle 12|\phi|1'2'\rangle$ of the form

$$\langle 12|\phi|1'2'\rangle = \delta_{1+2,1'+2'}\int dz \int dz' |\chi_1(z)|^2 |\chi_2(z')|^2 \times \phi(z,z',\mathbf{k}_1-\mathbf{k}_{1'}) . \tag{A1}$$

Here 1,2 and 1′,2′ are shorthand notations for the two-dimensional wave vectors $\mathbf{k}_1,\mathbf{k}_2$ and $\mathbf{k}_{1'},\mathbf{k}_{2'}$, with the subscript "1" referring to layer 1, and the subscript "2" referring to layer 2. The function $\phi(z,z',\mathbf{k}_1-\mathbf{k}_{1'})$ is the two-dimensional Fourier transform of the potential at z due to a test charge situated at z'.

Screening in heterostructures has been treated extensively in the literature (see e.g., Ref. 21). The Poisson equation for the potential $\phi(z,z')=\phi(z,z',\mathbf{k}_1-\mathbf{k}_{1'})$ is

$$\left[\frac{d^2}{dz^2}-q^2\right]\phi(z,z')=2q_{\rm TF}|\chi_1(z)|^2\phi_1(z')+2q_{\rm TF}|\chi_2(z)|^2\phi_2(z')-\frac{4\pi e}{\kappa}\delta(z-z') , \tag{A2}$$

where we have defined $\phi_i(z')$ by

$$\phi_i(z')=\int d\bar{z}|\chi_i(\bar{z})|^2\phi(\bar{z},z') . \tag{A3}$$

The solution of (A2), which requires the self-consistent determination of $\phi_1(z')$ and $\phi_2(z')$, may be conveniently performed by introducing the Green function $G(z-z')$ as a solution of the equation

$$\left[\frac{d^2}{dz^2}-q^2\right]G(z-z')=\delta(z-z') . \tag{A4}$$

It is readily verified that (A4) has the solution

$$G(z-z')=-\frac{1}{2q}e^{-q|z-z'|} . \tag{A5}$$

Therefore we have

$$\phi(z,z')=\int d\bar{z}\,G(z-\bar{z})\left[2q_{\rm TF}|\chi_1(\bar{z})|^2\phi_1(z')+2q_{\rm TF}|\chi_2(\bar{z})|^2\phi_2(z')-\frac{4\pi e}{\kappa}\delta(\bar{z}-z')\right] . \tag{A6}$$

We now introduce the definitions

$$G_i(z)=\int d\bar{z}\,G(z-\bar{z})|\chi_i(\bar{z})|^2 \tag{A7}$$

and

$$G_{ij}=\int dz\int dz'|\chi_i(z)|^2|\chi_j(z')|^2G(z-z') . \tag{A8}$$

This allows us to write (A6) in the compact form

$$\phi(z,z')=2q_{\rm TF}\phi_1(z')G_1(z)+2q_{\rm TF}G_2(z)\phi_2(z')-\frac{4\pi e}{\kappa}G(z-z') . \tag{A9}$$

It is now straightforward to determine ϕ_1 and ϕ_2 by multiplying (A9) by $|\chi_1(z)|^2$ and $|\chi_2(z)|^2$, respectively, and integrating over z. This yields

$$\phi_1(z')=-\frac{4\pi e}{\kappa}\frac{G_1(z')(1-2q_{\rm TF}G_{22})+2q_{\rm TF}G_{12}G_2(z')}{(1-2q_{\rm TF}G_{11})(1-2q_{\rm TF}G_{22})-4q_{\rm TF}^2G_{12}G_{21}} \tag{A10}$$

and

$$\phi_2(z')=-\frac{4\pi e}{\kappa}\frac{G_2(z')(1-2q_{\rm TF}G_{11})+2q_{\rm TF}G_{12}G_1(z')}{(1-2q_{\rm TF}G_{11})(1-2q_{\rm TF}G_{22})-4q_{\rm TF}^2G_{12}G_{21}} . \tag{A11}$$

The matrix element (A1) is therefore obtained by multiplying, e.g., $\phi_1(z')$ with $|\chi_2(z')|^2$ and integrating over z'. We get

$$\langle 12|\phi|1'2'\rangle=-\delta_{1+2,1'+2'}\frac{4\pi e}{\kappa}\frac{G_{21}(1-2q_{\rm TF}G_{22})+2q_{\rm TF}G_{12}G_{22}}{(1-2q_{\rm TF}G_{11})(1-2q_{\rm TF}G_{22})-4q_{\rm TF}^2G_{12}G_{21}} . \tag{A12}$$

Since $G_{12}=G_{21}$ this may be written in the simpler form

$$\langle 12|\phi|1'2'\rangle=\delta_{1+2,1'+2'}\phi(q) , \tag{A13}$$

where

$$\phi(q)=-\frac{4\pi e}{\kappa}\frac{G_{12}}{(1-2q_{\rm TF}G_{11})(1-2q_{\rm TF}G_{22})-4q_{\rm TF}^2G_{12}G_{21}} . \tag{A14}$$

In order to evaluate the form factors G_{ij} it is necessary to specify the form of the wave functions χ_i. We assume that the quantum wells are identical, and thus $G_{11}=G_{22}$. As an example, we shall take the wave functions χ_1 and χ_2 to have the form

$$\chi_1(z)=\begin{cases}\sqrt{2/L}\cos\dfrac{\pi z}{L} & \text{for } |z|<\dfrac{L}{2}\\ 0 & \text{for } |z|>\dfrac{L}{2}\end{cases} , \tag{A15}$$

while $\chi_2(z)$ is given by a similar expression, centered at $z=-d$. It is then straightforward to calculate G_{11} and G_{12}. We find

$$G_{12}=-\frac{1}{2q}e^{-qd}\left[\sinh\frac{qL}{2}\frac{8\pi^2}{qL(4\pi^2+q^2L^2)}\right]^2 , \tag{A16}$$

while

$$G_{11}=-\frac{1}{2q}\left[\frac{2}{qL}+\frac{qL}{4\pi^2+q^2L^2}-\left[\frac{8\pi^2}{qL(4\pi^2+q^2L^2)}\right]^2\sinh\frac{qL}{2}e^{-qL/2}\right]. \tag{A17}$$

In the limit $L\to 0$ the form factor G_{12} becomes equal to $-\exp(-qd)/2q$ while G_{11} becomes $-1/2q$. This is the limit in which the layers are treated as mathematical planes, corresponding to taking $|\chi_1(z)|^2=\delta(z)$ and $|\chi_2(z)|^2=\delta(z+d)$. If these expressions are inserted into (A14), one obtains

$$e\phi(q)=\frac{2\pi e^2}{\kappa}\frac{q}{2q_{\rm TF}^2\sinh qd+(2qq_{\rm TF}+q^2)\exp qd}, \tag{A18}$$

which is the result given in (29) of the main text.

*Also at Microelectronics Centre, Technical University of Denmark, 2800 Lyngby, Denmark.

[1]L. D. Landau and I. Pomeranchuk, Phys. Z. Sowjetunion **10**, 649 (1936).
[2]H. Smith and H. Højgaard Jensen, *Transport Phenomena* (Oxford University Press, New York, 1989).
[3]P. A. Lee and T. V. Ramakrishnan, Rev. Mod. Phys. **57**, 287 (1985).
[4]C. Hodges, H. Smith, and J. W. Wilkins, Phys. Rev. B **4**, 302 (1971).
[5]A. V. Chaplik, Zh. Eksp. Teor. Fiz. **60**, 1845 (1971) [Sov. Phys. JETP **33**, 997 (1971)].
[6]A. Yacoby, U. Sivan, C. P. Umbach, and J. M. Hong, Phys. Rev. Lett. **66**, 1938 (1991).
[7]T. J. Gramila, J. P. Eisenstein, A. H. MacDonald, L. N. Pfeiffer, and K. W. West, Phys. Rev. Lett. **66**, 1216 (1991).
[8]T. J. Gramila, J. P. Eisenstein, A. H. MacDonald, L. N. Pfeiffer, and K. W. West (unpublished).
[9]P. J. Price, Physica B **117**, 750 (1983).
[10]M. B. Pogrebinskii, Fiz. Tekh. Poluprovodn. **11**, 637 (1977) [Sov. Phys. Semicond. **11**, 372 (1977)].
[11]B. Laikhtman and P. M. Solomon, Phys. Rev. B **41**, 9921 (1990).
[12]P. M. Solomon and B. Laikhtman, Superlatt. Microstruct. B **10**, 89 (1991).
[13]I. I. Boiko and Yu. M. Sirenko, Phys. Status Solidi **159**, 805 (1990).
[14]A. G. Rojo and G. D. Mahan, Phys. Rev. Lett. **68**, 2074 (1992).
[15]D. I. Maslov, Phys. Rev. B **45**, 1911 (1992).
[16]H. C. Tso and P. Vasilopoulos, Phys. Rev. B **45**, 1333 (1992).
[17]U. Sivan, P. M. Solomon, and H. Shtrikman, Phys. Rev. Lett. **68**, 1196 (1992).
[18]G. F. Giuliani and J. J. Quinn, Phys. Rev. B **26**, 4421 (1982).
[19]P. F. Maldague, Surf. Sci. **73**, 296 (1978).
[20]The slight irregularities seen in Fig. 2 are an artifact of the graphics routine which we employ, and in reality the integrand is smooth. The sharp ridge requires a large number of mesh points in the numerical integration, and typically 140 000 function evaluations are needed to reach convergence.
[21]T. Ando, A. B. Fowler, and F. Stern, Rev. Mod. Phys. **54**, 437 (1982).